Supplement of Atmos. Chem. Phys., 26, 10927–10946, 2026
https://doi.org/10.5194/acp-26-10927-2026-supplement

Supplement of

Measurement report: Evolving sources and composition of urban submicron aerosols in Dublin: impacts of emission reductions and transboundary transport

Lu Lei et al.

Correspondence to: Lu Lei (lu.lei@universityofgalway.ie) and Jurgita Ovadnevaite (jurgita.ovadnevaite@universityofgalway.ie)

S1.1 Reconstruction of missing eBC data and evaluation of associated uncertainty

Due to instrumental issues, eBC measurements were not available between 2018 and 2020. To maintain a continuous dataset for long-term trend analysis, eBC mass concentrations during these periods were reconstructed from concurrent OA mass concentrations using a single annual mean eBC/OA ratio of 0.24. This ratio was derived from all periods with valid eBC measurements, including 2016-2017 and 2021-2023. The use of the OA-based reconstruction is supported by the generally similar temporal variations of eBC and OA in urban Dublin, their strong correlations and relatively stable mass ratios during periods with valid measurements (Table S1), reflecting their common sources.

To evaluate the uncertainty associated with this reconstruction, we first assessed the potential influence of seasonal variability in the eBC/OA ratio. Monthly mean eBC/OA ratios were calculated from all available measured eBC data. As shown in Fig. S10a, the eBC/OA ratio shows clear seasonal variability, with lower values in summer and higher values during colder months. As a result, the coefficient of variation of the monthly mean eBC/OA ratios was 22% (CV = standard deviation / mean × 100 %), indicating moderate seasonal variability in the eBC/OA relationship. We therefore compared the original reconstruction based on the single annual mean ratio with an alternative reconstruction using monthly eBC/OA ratios. The two methods produced generally similar reconstructed eBC values, although the monthly-ratio method showed slightly better agreement with the measured eBC (Fig. S10b-d). The reconstruction performance was relatively weaker for 2016-2017, likely due to the lower eBC-OA correlation and higher eBC/OA ratio during this period compared with 2021-2023, suggesting potential interannual uncertainty in the eBC reconstruction.

We then examined whether the choice of reconstruction method affected the long-term eBC trend. The annual mean eBC trend was nearly identical between the two methods: the Mann-Kendall trend significance remained unchanged, and the fitted slope was -0.07 $\mu g\ m^{-3}\ yr^{-1}$ for both reconstructions. For the yearly maximum hourly eBC concentration, the fitted slope changed only from -12.6 to -11.7 $\mu g\ m^{-3}\ yr^{-1}$ when monthly ratios were used, corresponding to a relative difference of less than 10 %. These results indicate that, although the eBC/OA ratio shows measurable seasonal variability, the use of a single annual mean eBC/OA ratio has only a limited influence on the long-term eBC trend conclusions.

As a second sensitivity test, we repeated the eBC trend analysis after excluding the reconstructed eBC data for 2018 and 2020 and using only directly measured eBC data. The decreasing trend remained significant ($p < 0.05$), and the fitted slope was very similar to that obtained when the reconstructed data were included (-0.06 vs. -0.07 $\mu g\ m^{-3}\ yr^{-1}$; Table S3). This indicates that the long-term decreasing eBC trend is not significantly biased by the OA-based reconstruction. Overall, these sensitivity tests support the robustness of the long-term eBC trend, although the fitted magnitude of the eBC trend remains subject to greater uncertainty than trends derived entirely from directly measured components.

S1.2 Influence of long-term concentration changes on seasonal patterns

To assess whether the long-term decreases in PM_1 components affected the overall seasonal characteristics, monthly variations in PM_1 composition were compared between the early period (2016-2018) and the later period after the substantial concentration decrease observed from 2021 onwards (2021-2023).

As shown in Fig. S15, differences were observed between the two periods, particularly in terms of absolute concentrations, as expected from the long-term trends and potential interannual variability. For example, during 2016-2018, PM_1 showed a pronounced enhancement in October, with a monthly mean concentration even higher than that in January (8.0 vs. 7.0 $\mu g\ m^{-3}$), mainly driven by stronger local domestic heating emissions. In contrast, during 2021-2023, although PM_1 concentrations remained elevated in the coldest months (Dec.-Jan., > 6 $\mu g\ m^{-3}$), the highest monthly PM_1 concentrations occurred in March-April (6.6-7.5 $\mu g\ m^{-3}$). Overall, PM_1 concentrations during 2021-2023 were lower than those during 2016-2018, especially in colder months (4.6-6.4 vs. 7.2-12.4 $\mu g\ m^{-3}$), and the contrast between cold-season and other months became less pronounced. This is consistent with the long-term decreases in local home heating-related components, including eBC, solid fuel OA, HOA, and OOA_{local}, as discussed in the main trend analysis.

Despite these differences, the dominant seasonal features remained clear and broadly consistent between the two periods. More specifically, PM_1 concentrations were generally enhanced during colder months, particularly in January, November, and December, and in some cases also during the transitional month of October. These cold season enhancements were mainly associated with local domestic heating emissions, as reflected by the increased contributions of locally emitted components. Spring, especially March-April, remained the period most strongly influenced by transboundary transport, with the highest relative contributions of NO_3 (24-25% in 2016-2018 and 21-23% in 2021-2023) and enhanced contributions of NH_4 and OOA_{TBT}. This regional influence could also extend into May. By contrast, the summer months, especially June-September, consistently represented the cleanest period, with relatively low PM_1 and OA concentrations and a larger relative contribution from secondary components.

Overall, the comparison shows that the long-term decreases in PM_1 components affected the absolute concentration levels and introduced some differences in the monthly patterns between the early and later periods. However, the main seasonal structure was largely preserved: colder months were mainly influenced by local domestic heating emissions, spring was more strongly affected by transboundary transport, and summer remained the cleanest period.

Table S1. Mass ratios (eBC/OA) and correlation coefficients (r^2) between eBC and OA for each year when eBC data was available from 2016 to 2023.

Year	eBC/OA	r^2
2016-2017	0.31	0.76
2018	-	-
2019	-	-
2020	-	-
2021	0.18	0.88
2022	0.22	0.83
2023	0.26	0.86

Table S2. Summary of the number of polluted days dominated by local home heating emissions, transboundary transport (TBT), or mixed influences in each year.

Year	Local-dominated	TBT-dominated	Mixed
2016-2017	19	7	5
2018	19	6	5
2019	18	0	6
2020	13	6	2
2021	10	7	3
2022	9	4	8 (3*)
2023	8	1	1

***Three of the eight mixed events showed less typical pollution characteristics, with a high SO_4 fraction.**

Table S3. Comparison of long-term eBC trends using different treatments for the missing eBC data between 2018 and 2020, including reconstruction with a single annual mean eBC/OA ratio, reconstruction with monthly mean eBC/OA ratios, and exclusion of the missing data periods. The Mann-Kendall test results and fitted linear slopes, together with the 95 % confidence intervals, are shown for both annual mean eBC mass concentration and yearly maximum hourly eBC concentration.

Methods	P-value	Slope (95% CI) ($\mu g\ m^{-3}\ yr^{-1}$)	Slope of annual hourly maxima* (95% CI) ($\mu g\ m^{-3}\ yr^{-1}$)
Annual eBC/OA	<0.05	-0.07 (-0.10 – -0.04)	-12.6 (-19.1 – -6.0)
Monthly eBC/OA	<0.05	-0.07 (-0.09 – -0.04)	-11.7 (-20.8 – -2.7)
2018 and 2020 excluded	<0.05	-0.06 (-0.10 – -0.01)	-9.5 (-18.4 – -0.9)

Table S4. Mann-Kendall test results for gaseous pollutants from 2016 to 2023, along with linear regression slopes and the 95% confidence intervals based on annual average mass concentrations. The upward arrows denote increasing trends, downward arrows denote decreasing trends, and the absence of arrows indicates non-significant trends ($p > 0.05$).

Species	P-value	Slope (95% CI) ($\mu g\ m^{-3}\ yr^{-1}$)
SO_2	<0.05	0.05 (-0.30 – 0.40)↑
NO_2	<0.05	-1.16 (-2.80 – 0.49)↓
O_3	<0.05	2.21 (-0.11 – 4.53)↑

Table S5. Comparison of Mann-Kendall test results and fitted slopes for major PM_1 species using the full dataset and a sensitivity dataset excluding the COVID-19 affected years (2020 and 2021).

Species	P-value (20-21 excluded)	Slope (95% CI) ($\mu g\ m^{-3}\ yr^{-1}$) (20-21 excluded)	P-value (all years)	Slope (95% CI) ($\mu g\ m^{-3}\ yr^{-1}$) (all years)
PM_1	<0.05	-0.42 (-0.65 – -0.19)	<0.05	-0.46 (-0.70 – -0.23)
Org	0.14	-0.13 (-0.42 – 0.18)	0.20	-0.14 (-0.34 – 0.06)
SO_4	<0.05	-0.03 (-0.08 – 0.02)	0.06	-0.04 (-0.09 – 0.02)
NO_3	<0.05	-0.09 (-0.14 – -0.03)	<0.05	-0.11 (-0.18 – -0.03)
NH_4	<0.05	-0.08 (-0.13 – -0.02)	<0.05	-0.09 (-0.16 – -0.03)
eBC	<0.05	-0.06 (-0.09 – -0.03)	<0.05	-0.07 (-0.10 – -0.04)
Solid fuel OA	<0.05	-0.07 (-0.20 – 0.06)	<0.05	-0.08 (-0.16 – -0.02)
HOA	<0.05	-0.03 (-0.05 – -0.01)	<0.05	-0.04 (-0.06 – -0.02)
OOA_{local}	0.89	-0.02 (-0.14 – 0.08)	0.64	-0.03 (-0.10 – 0.03)
OOA_{TBT}	<0.05	0.02 (-0.01 – 0.05)	<0.05	0.02 (-0.08 – 0.13)

Table S6. Mann-Kendall test results for gaseous pollutants from 2016 to 2023, along with linear regression slopes and the 95% confidence intervals based on annual average mass concentrations under low ($PM_1 < 15$ µg m^{-3}), moderate ($15 \leq PM_1 < 50$ µg m^{-3}) and high pollution ($PM_1 \geq 50$ µg m^{-3}) conditions. The upward arrows denote increasing trends, downward arrows denote decreasing trends, and the absence of arrows indicates non-significant trends ($p > 0.05$).

Species	P-value (Low)	Slope (95% CI) (µg m^{-3} yr^{-1})	P-value (Moderate)	Slope (95% CI) (µg m^{-3} yr^{-1})	P-value (High)	Slope (95% CI) (µg m^{-3} yr^{-1})
SO_2	<0.05	0.09 (-0.27 – 0.45)↑	<0.05	-0.01 (-0.36 – 0.34)↓	<0.05	-0.44 (-1.74 – 0.88)↓
NO_2	<0.05	-0.90 (-2.60 – 0.79)↓	<0.05	-1.14 (-3.68 – 1.41)↓	<0.05	-2.30 (-5.23 – 0.70)↓
O_3	<0.05	1.97 (-0.41 – 4.35)↑	<0.05	1.13 (-4.34 – 6.60)↑	<0.05	0.84 (-0.80 – 2.49)↑

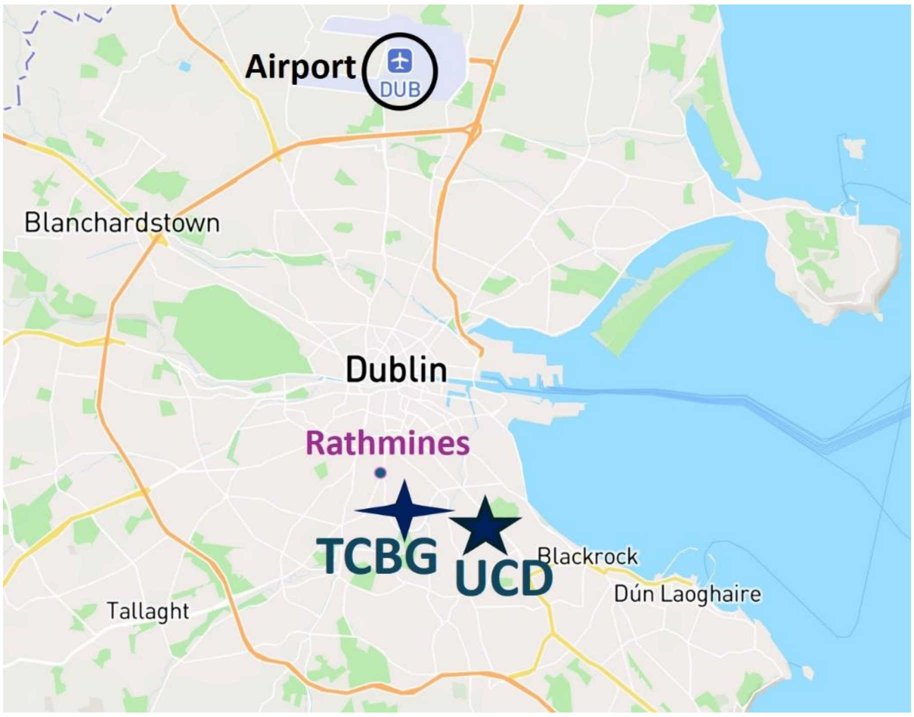

Figure S1. Locations of the original UCD site, the new TCBG site, the EPA Rathmines monitoring station, and Dublin Airport, where meteorological parameters were recorded. Map data © 2025 Google.

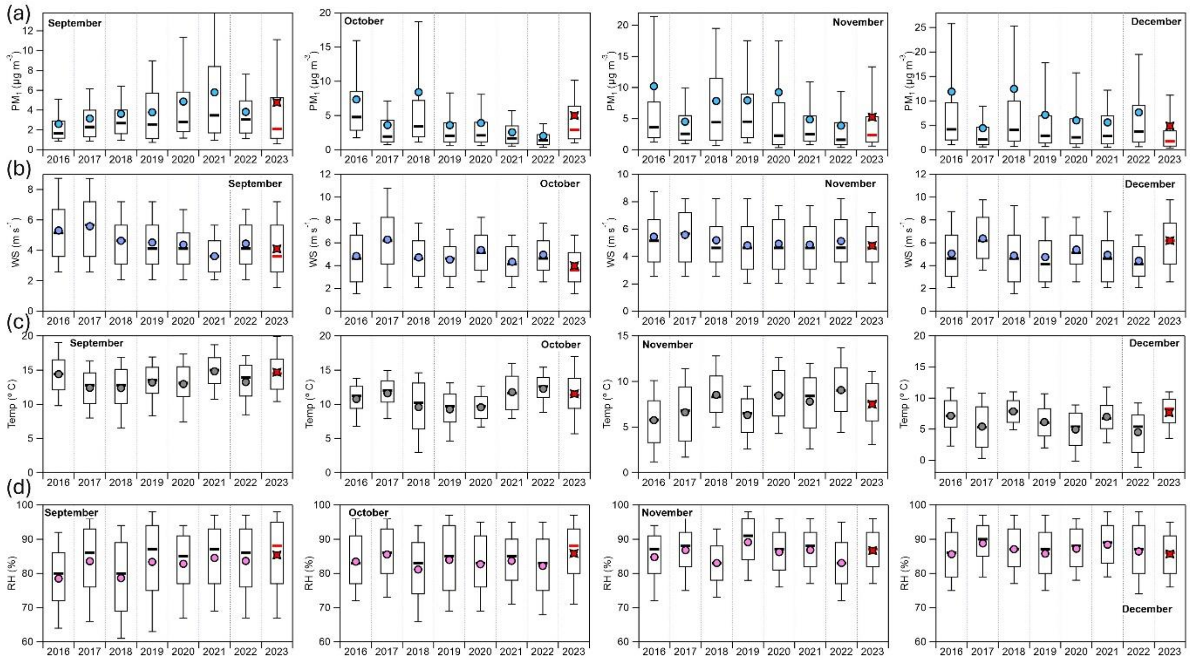

Figure S2. Box plots comparing total PM$_1$ mass concentrations from September to December between the original UCD site (2016-2022) and the relocated TCBG site (2023). Corresponding box plots of meteorological parameters, including (b) wind speed (WS), (c) ambient temperature (Temp), and (d) relative humidity (RH), are also shown to assess interannual variability and support the comparability of long-term data across the two sites. The mean (circle), median (horizontal line), 25th-75th percentiles (box), and 10th-90th percentiles (whiskers) are shown. Note that meteorological data for both sites originate from Dublin Airport, thus, the box plots illustrate interannual meteorological variability rather than differences between the two measurement locations. The slightly higher PM$_1$ concentration at the new TCBG site may be explained by the relatively low wind speeds in October 2023 compared with previous years.

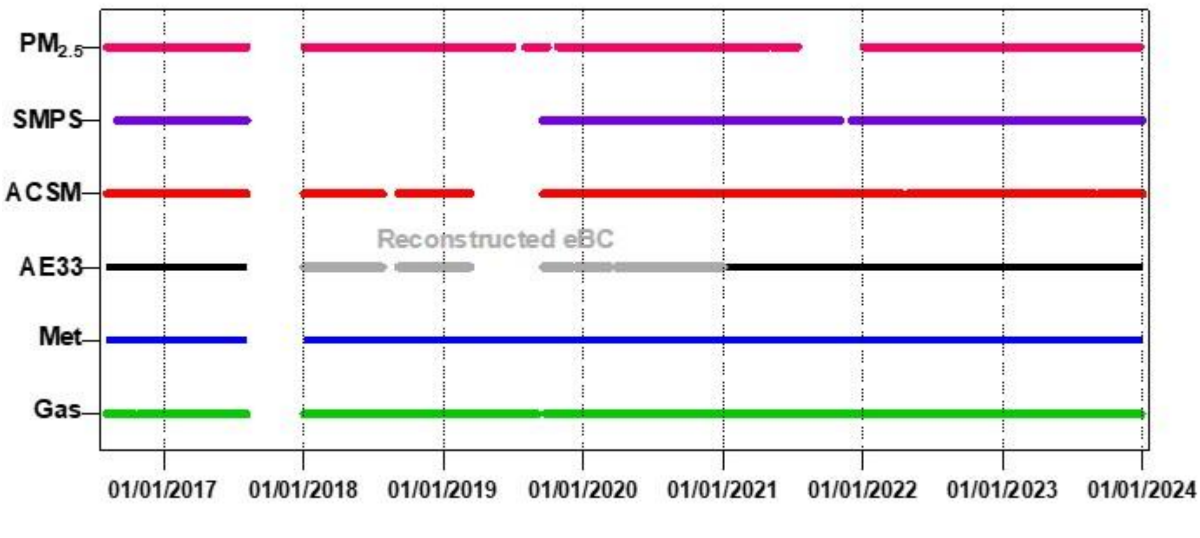

Figure S3. Hourly data coverage for PM$_{2.5}$ concentrations and measurements from SMPS, ACSM (for PM$_1$ chemical species), AE33 (for eBC), as well as meteorological parameters and trace gases, from 2016 to 2023 in Dublin.

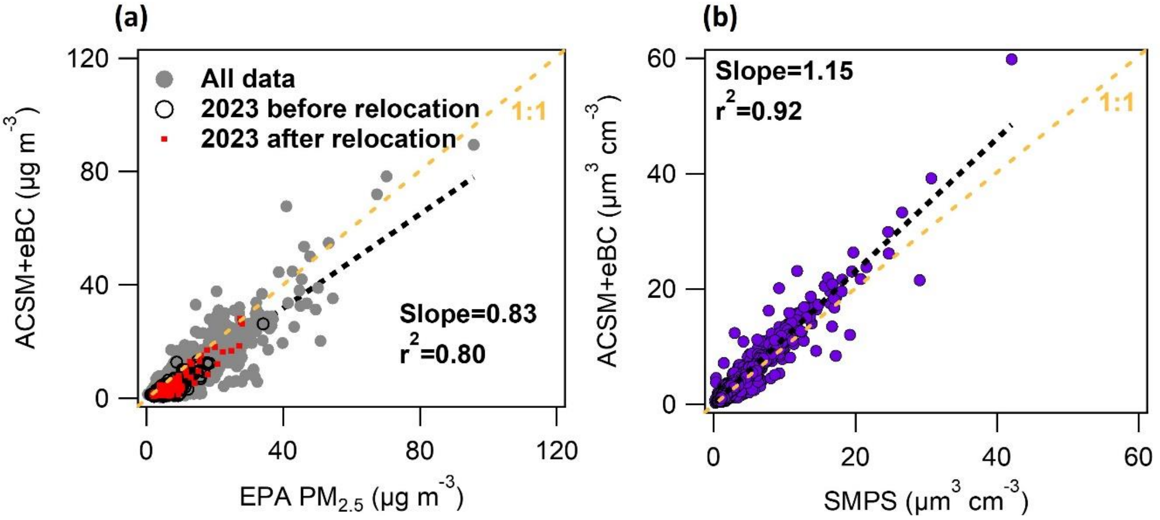

Figure S4. Scatter plots comparing multi-year PM_1 measurements (Q-ACSM + AE33, i.e., NR-PM_1 + eBC) in Dublin from 2016 to 2023 with (a) $PM_{2.5}$ concentrations from the Rathmines monitoring station and (b) particle volume concentrations from the collocated SMPS system. In panel (a), black open circles denote data from January to August 2023 (before site relocation), and red dots represent data from September to December 2023 (after relocation). The $PM_1/PM_{2.5}$ ratios show no systematic change across the two periods, indicating that the site relocation did not affect the consistency of the measurements.

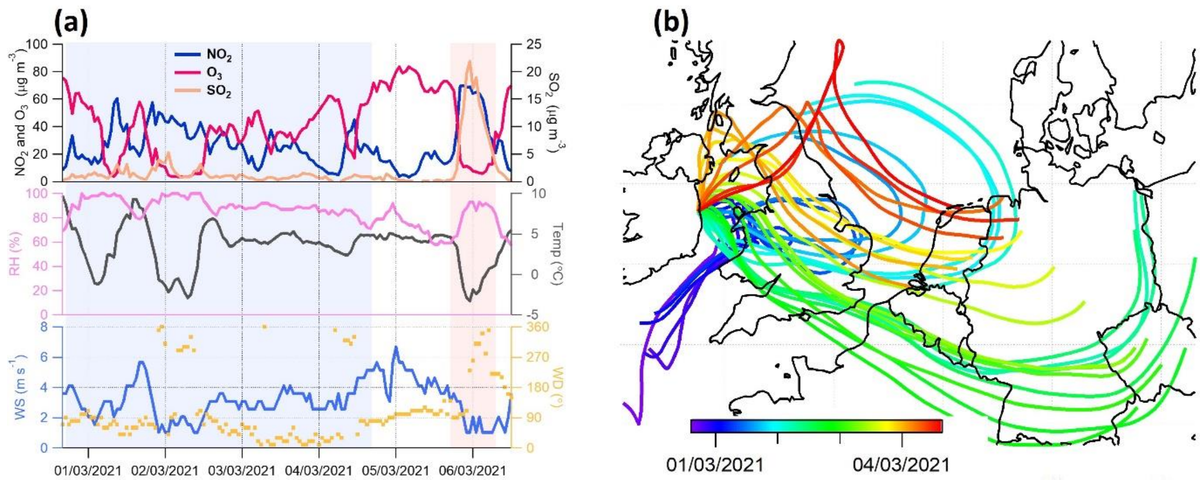

Figure S5. (a) Time series of meteorological parameters, including wind speed (WS), wind direction (WD), ambient temperature, relative humidity (RH), and gaseous pollutants (NO_2, SO_2, and O_3), during two representative pollution episodes dominated by transboundary transport (left, light blue shading) and local emissions (right, light pink shading). (b) 72-hour backward air mass trajectories during the transboundary transport episode, illustrating the regional origin of the polluted air masses.

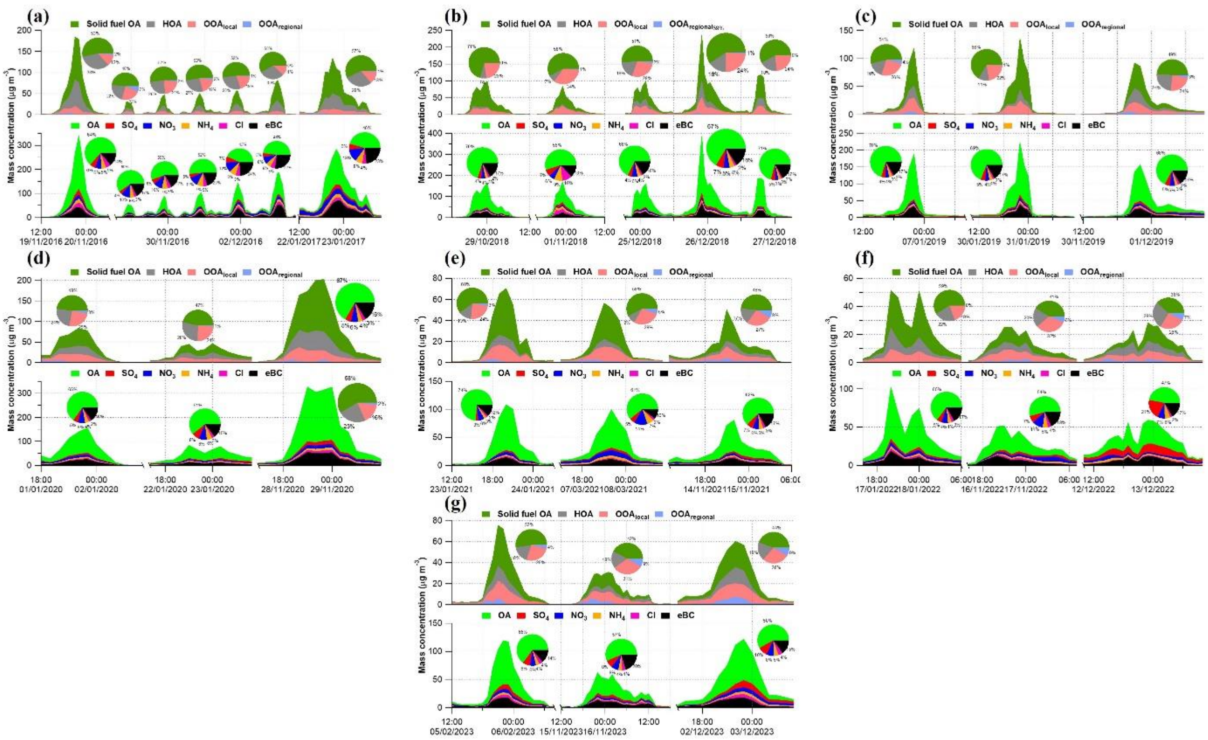

Figure S6. Examples of local home heating dominated pollution events in each year from 2016 to 2023. The examples correspond to the three polluted days with the highest daily mean PM_1 mass concentrations in each year, including adjacent continuous event periods before or after the selected polluted days where applicable.

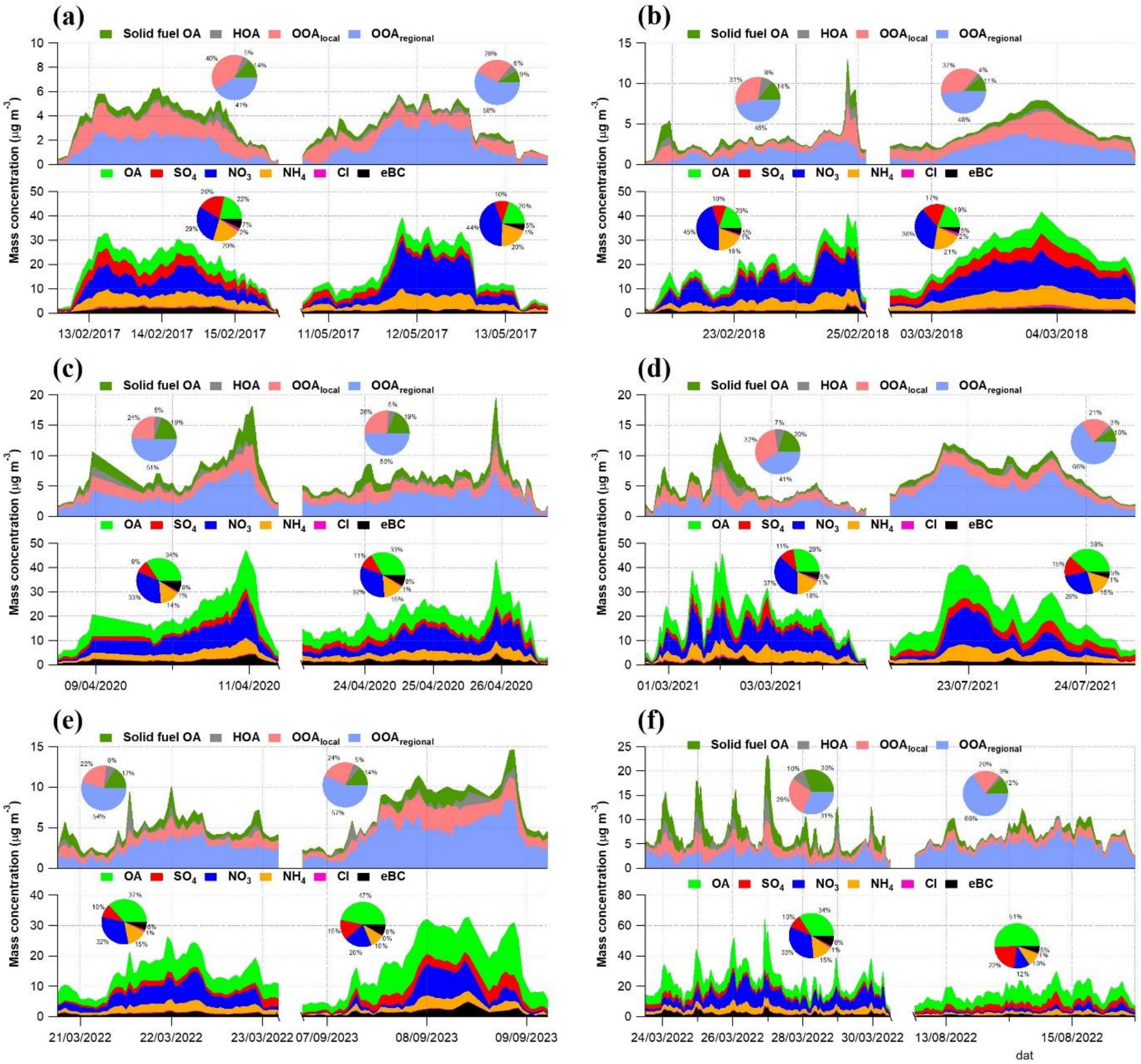

Figure S7. Examples of transboundary transport dominated pollution events from 2016 to 2023. The examples correspond to polluted days with daily mean PM_1 mass concentrations above 20 µg m^{-3} in each year, where available. One example each of a mixed event and a less typical event is also shown in panel (f).

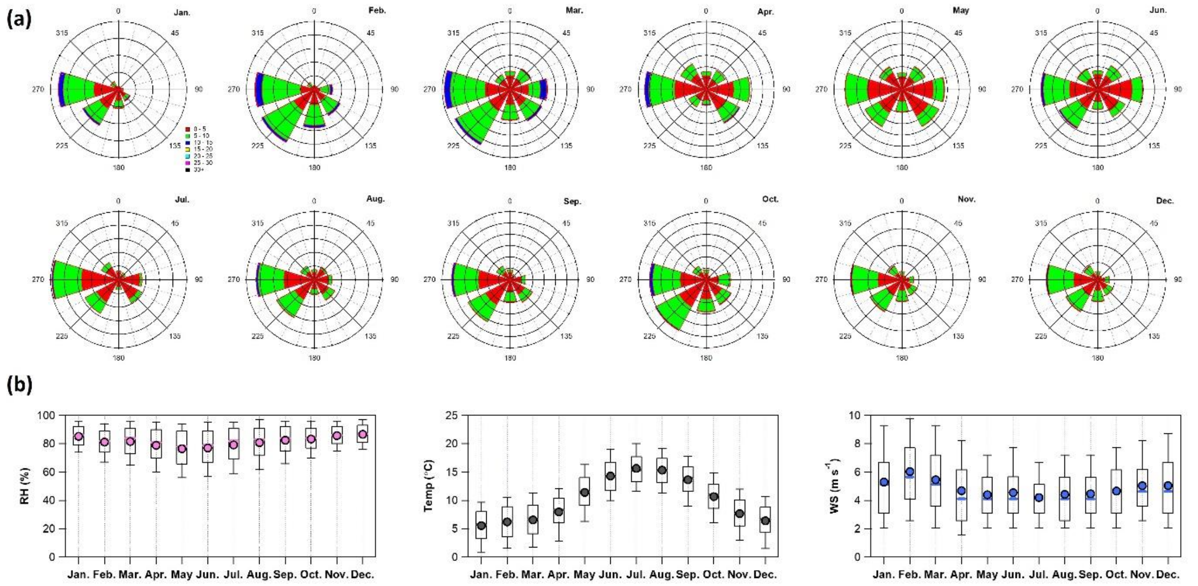

Figure S8. (a) Monthly average wind rose plots from January to December, and (b) box plots of monthly relative humidity (RH), ambient temperature, and wind speed (WS) based on data from 2016 to 2023 in Dublin.

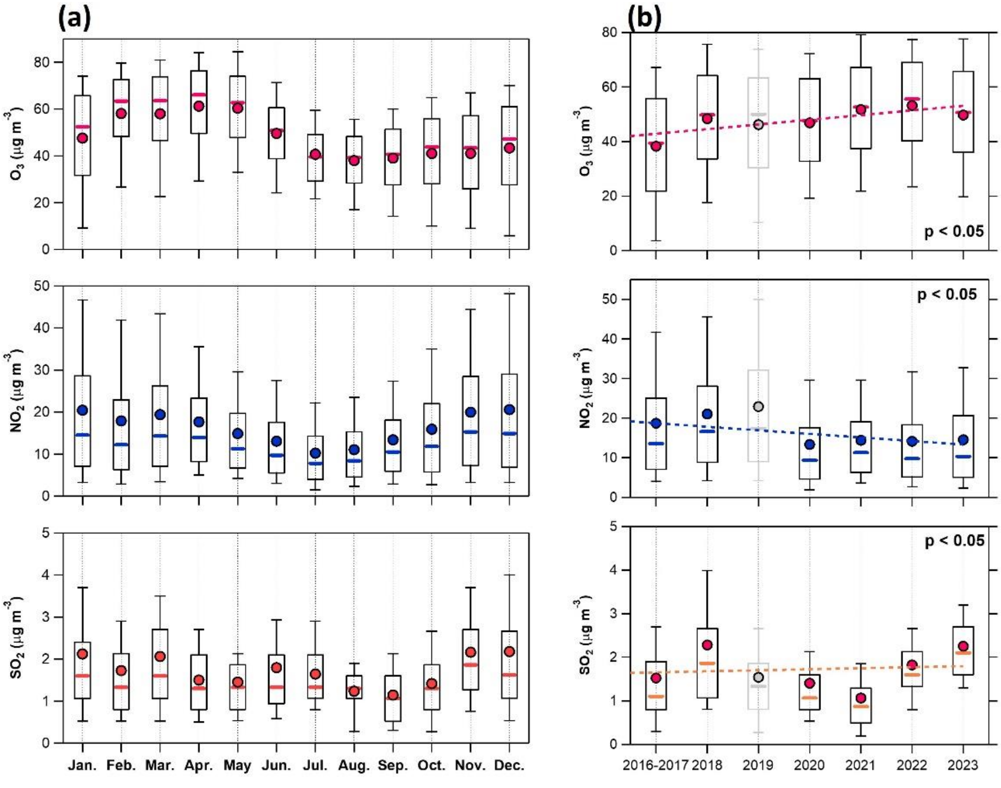

Figure S9. Box plots of (a) monthly mean and (b) annual mean concentrations of gaseous pollutants (O_3, NO_2, and SO_2) in Dublin from 2016 to 2023. The mean (circle), median (horizontal line), 25th-75th percentiles (box), and 10th-90th percentiles (whiskers) are shown. Please note that 2019 is excluded from long-term trend analysis and is shown in grey due to biased data coverage.

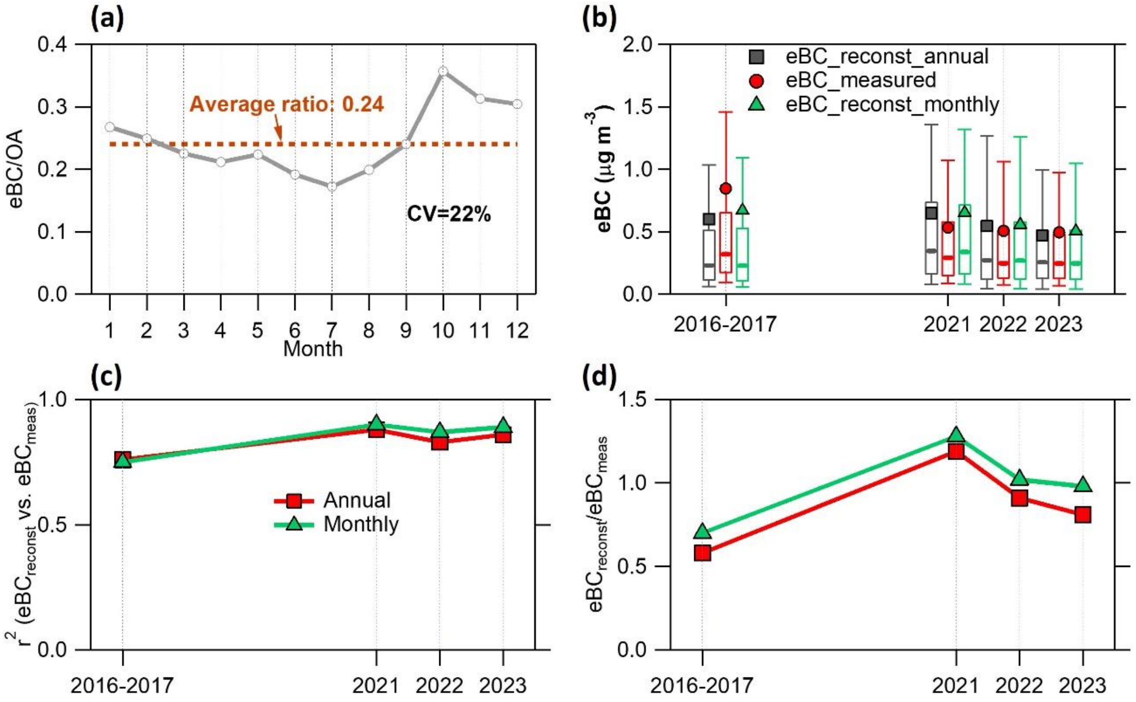

Figure S10. Monthly mean eBC/OA mass ratios calculated from all available eBC measurements in 2016-2017, 2021, 2022, and 2023. The annual mean eBC/OA ratio and the corresponding coefficient of variation (CV = standard deviation / mean × 100 %) of the monthly ratios are also shown. Panels b-d compare the reconstructed eBC with the measured eBC using either a single annual eBC/OA ratio or monthly eBC/OA ratios, showing box plots of the overall distributions, fitted slopes and correlation coefficients (r^2), respectively.

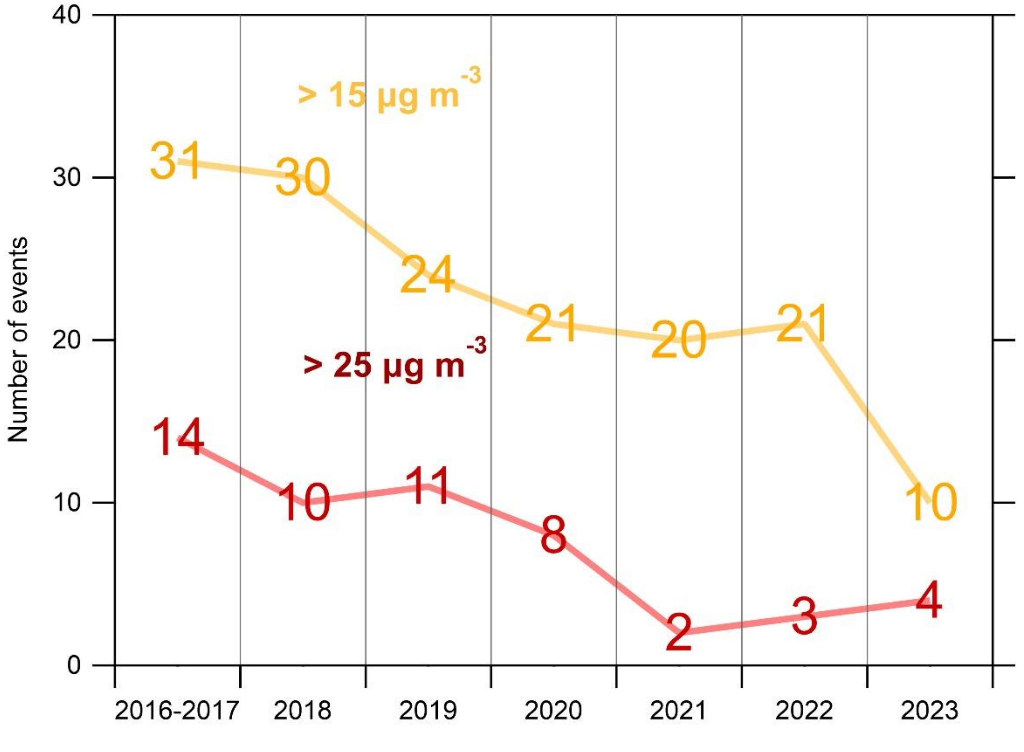

Figure S11. Long-term trends in the number of polluted days (daily PM_1 > 15 μg m^{-3}) in Dublin from 2016 to 2023. The orange line marks the current WHO daily guideline (15 μg m^{-3}), while the red line indicates the previous guideline (25 μg m^{-3}).

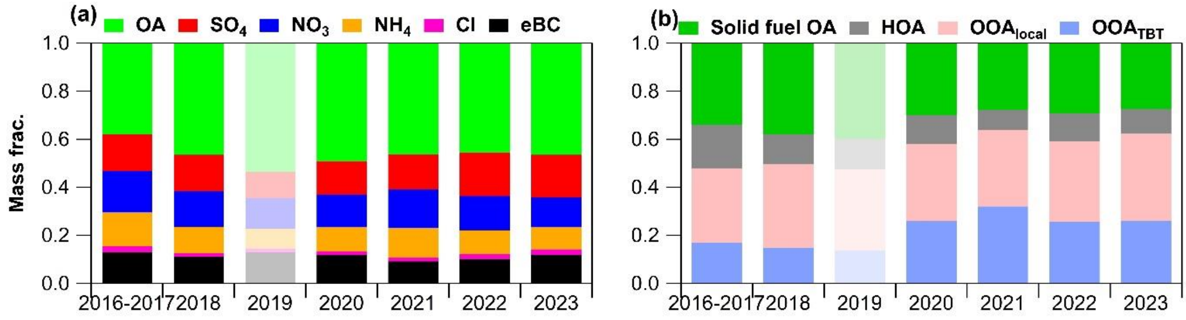

Figure S12. Annual average composition of PM$_1$ and OA from 2016 to 2023. Data for 2019 are excluded from long-term comparisons due to limited coverage and are shown in grey for reference.

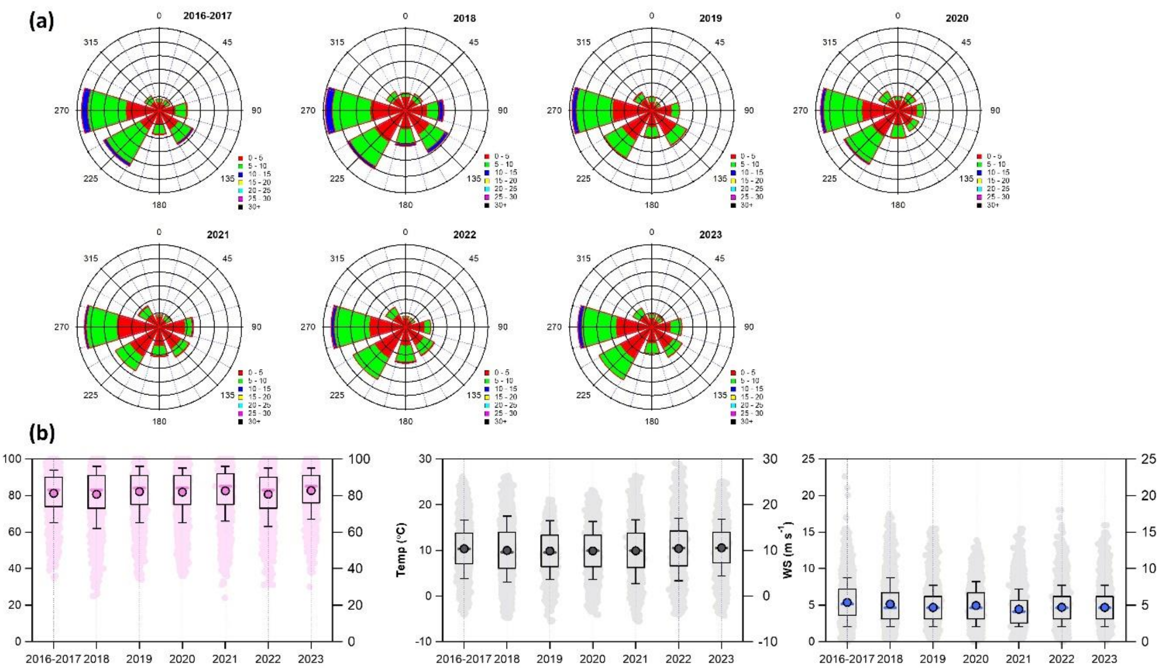

Figure S13. (a) Annual average wind rose plots, and (b) box plots of annual relative humidity (RH), ambient temperature, and wind speed (WS) based on data from 2016 to 2023 in Dublin.

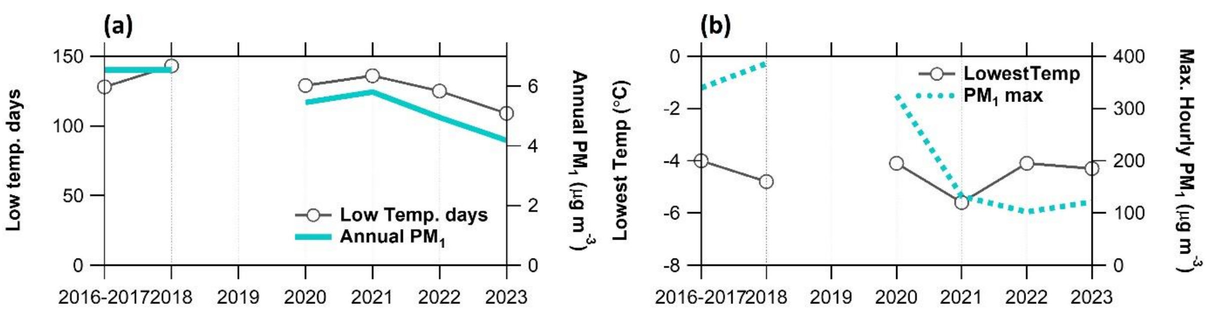

Figure S14. Long-term trends in (a) low-temperature days (daily minimum < 5 °C) and (b) annual minimum temperature from 2016 to 2023 (excluding 2019). Annual average and maximum PM$_1$ concentrations are also shown.

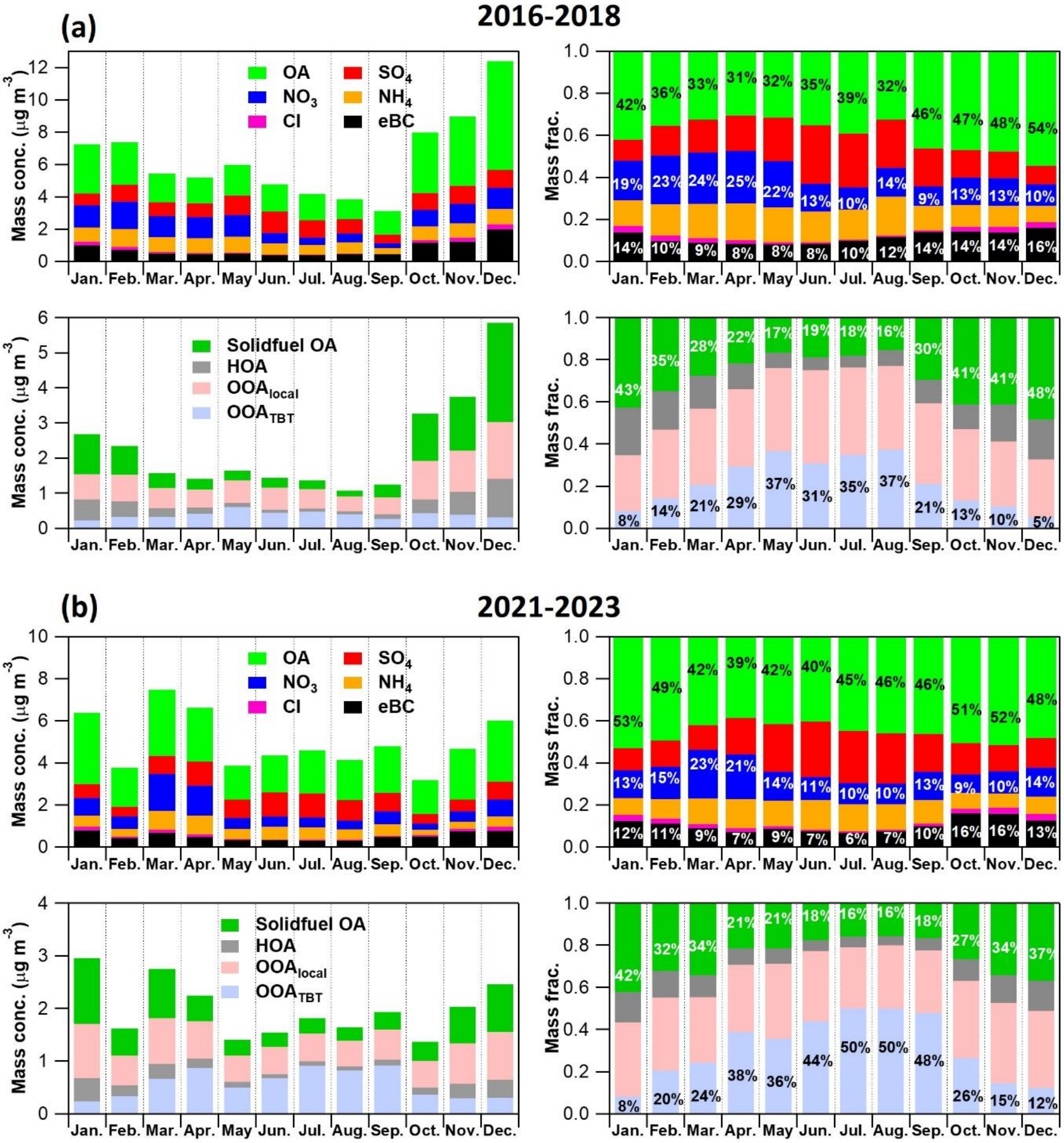

Figure S15. Comparison of monthly mean PM_1 and OA mass concentrations and chemical composition in Dublin between 2016-2018 and 2021-2023. The percentage contributions of major PM_1 and OA components are shown.

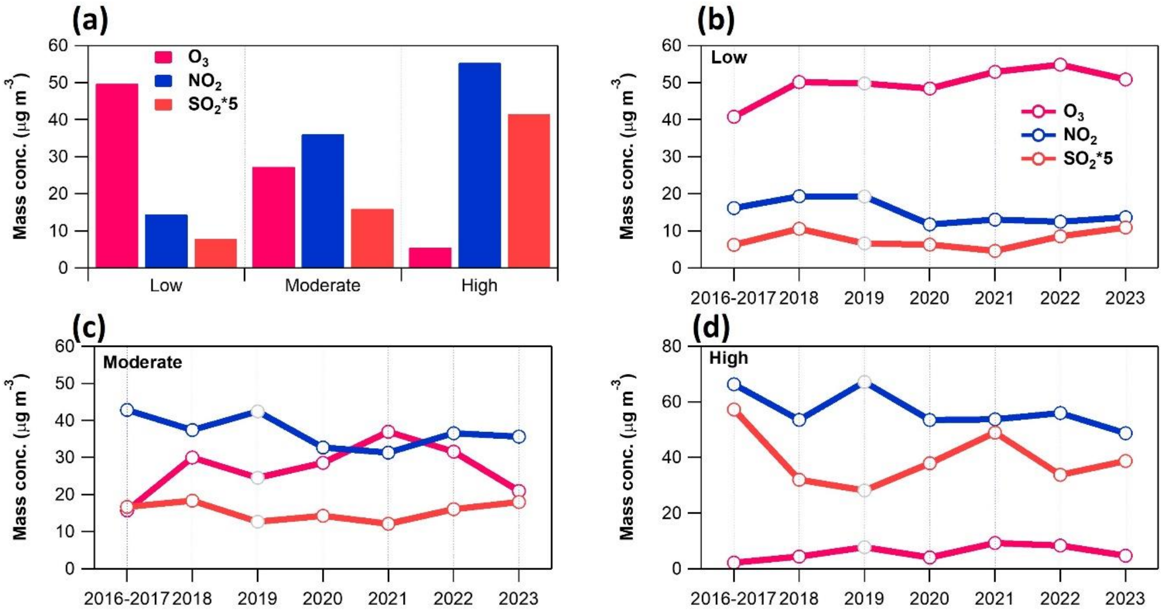

Figure S16. (a) Average concentrations of gaseous pollutants and (b-d) their long-term trends based on annual means under low, moderate, and high pollution levels from 2016 to 2023.

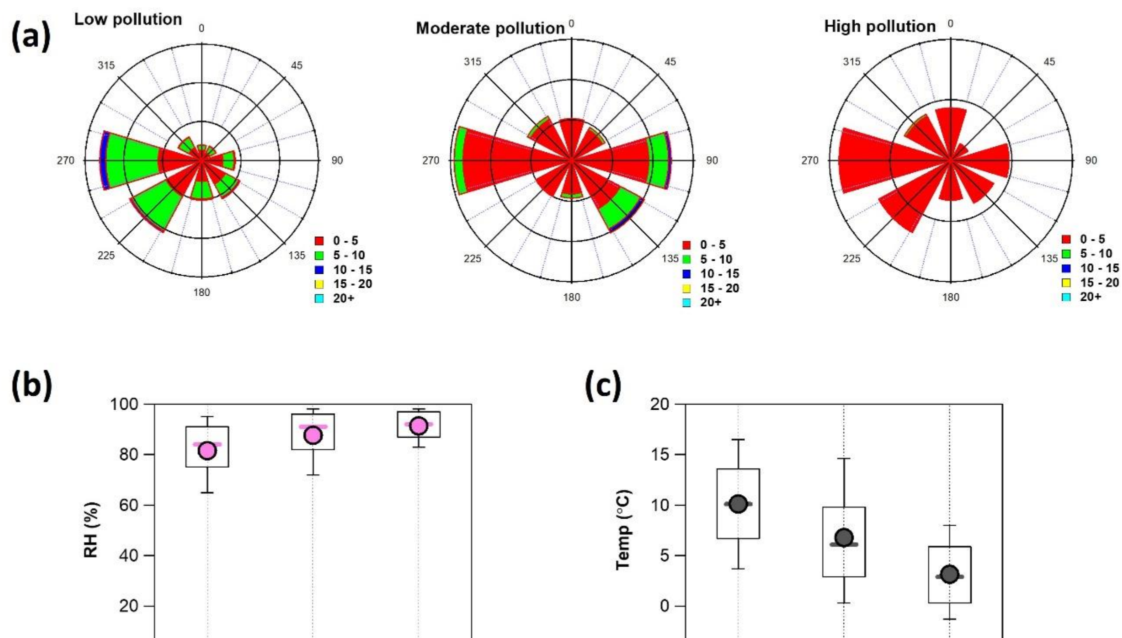

Figure S17. (a) Wind rose plots and box plots of (b) relative humidity (RH) and (c) ambient temperature (Temp) under low, moderate, and high pollution conditions. Higher pollution levels are generally associated with more stagnant meteorological conditions, including lower wind speeds and Temp, and elevated RH.

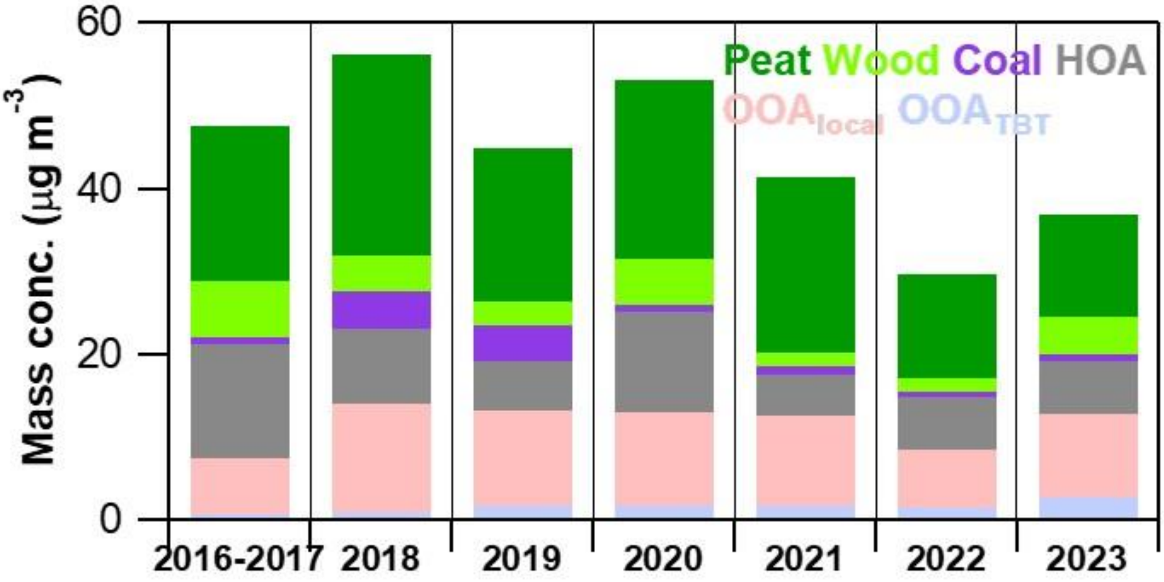

Figure S18. Long-term trends of detailed OA factors, including peat, wood, coal, HOA, OOA_{local}, and OOA_{TBT} under high pollution conditions in Dublin from 2016 to 2023.